ADVANCED MATERIALS
www.advmat.de

Signatures of Sixfold Degenerate Exotic Fermions in a Superconducting Metal $PdSb_2$

Nitesh Kumar, Mengyu Yao, Jayita Nayak, Maia G. Vergniory, Jörn Bannies, Zhijun Wang, Niels B. M. Schröter, Vladimir N. Strocov, Lukas Müchler, Wujun Shi, Emile D. L. Rienks, J. L. Mañes, Chandra Shekhar, Stuart S. P. Parkin, Jörg Fink, Gerhard H. Fecher, Yan Sun, B. Andrei Bernevig, and Claudia Felser**

Multifold degenerate points in the electronic structure of metals lead to exotic behaviors. These range from twofold and fourfold degenerate Weyl and Dirac points, respectively, to sixfold and eightfold degenerate points that are predicted to give rise, under modest magnetic fields or strain, to topological semimetallic behaviors. The present study shows that the nonsymmorphic compound $PdSb_2$ hosts six-component fermions or sextuplets. Using angle-resolved photoemission spectroscopy, crossing points formed by three twofold degenerate parabolic bands are directly observed at the corner of the Brillouin zone. The group theory analysis proves that under weak spin–orbit interaction, a band inversion occurs.

Condensed matter systems can exhibit quasiparticle excitations which mimic the wavefunctions of exotic fermions predicted in high energy physics.[1] For example, Dirac and Weyl fermions exist as low energy electronic excitations of several semimetals near the Dirac points and Weyl points.[2–9] While Dirac points are fourfold degenerate, Weyl points are twofold degenerate and always appear in pairs.[10] The linear dispersive bands and the surface Fermi arc states around these points have been shown to lead to exotic transport properties, such as large carrier mobility,[11,12] anomalous Hall conductivity,[13–15] a chiral anomaly–induced negative magnetoresistance,[16–18] and a 3D quantum Hall effect.[19,20] More importantly, condensed matter systems can realize novel fermions which have otherwise no counterpart in high energy physics[21] because the former do not need to follow certain symmetries which are mandatory for the latter. Bradlyn et al. discovered that one can find threefold, sixfold, or eightfold degenerate symmetry protected points in many compounds.[22] While the threefold points can be realized in both nonsymmorphic[22,23] and symmorphic crystal structures,[23] nonsymmorphic operations are essential for stabilizing sixfold and eightfold degenerate points. Threefold degenerate points, also known as triple points, were observed in MoP[24] and WC.[25] The sixfold degenerate points, which we call sextuple points, have been recently observed experimentally in the chiral compound CoSi, RhSi, and AlPt in the space group $P2_13$ (198).[26–28] However, the latter study was mainly

Dr. N. Kumar, Dr. M. Yao, Dr. J. Nayak, J. Bannies, Dr. L. Müchler, Dr. W. Shi, Dr. C. Shekhar, Prof. J. Fink, Dr. G. H. Fecher, Dr. Y. Sun, Prof. C. Felser
Max Planck Institute for Chemical Physics of Solids
Nöthnitzer Str. 40, 01187 Dresden, Germany
E-mail: Nitesh.Kumar@cpfs.mpg.de; Claudia.Felser@cpfs.mpg.de

Dr. M. G. Vergniory
Donostian International Physics Center
Paseo Manuel de Lardizabal 4, 20018 San Sebastian, Spain

Dr. M. G. Vergniory
KERBASQUE
Basque Foundation for Science
Maria Diaz de Haro 3, 48013 Bilbao, Spain

Dr. Z. Wang, Prof. B. A. Bernevig
Department of Physics
Princeton University
Princeton, NJ 08544, USA

The ORCID identification number(s) for the author(s) of this article can be found under https://doi.org/10.1002/adma.201906046.

DOI: 10.1002/adma.201906046

Dr. N. B. M. Schröter, Dr. V. N. Strocov
Paul Scherrer Institute
5232 Villigen, PSI, Switzerland

Dr. L. Müchler
Center for Computational Quantum Physics
The Flatiron Institute
New York, NY 10010, USA

Dr. E. D. L. Rienks, Prof. J. Fink
Leibniz Institut für Festkörper und Werkstoffforschung IFW Dresden
Helmholtzstrasse 20, 01171 Dresden, Germany

Dr. E. D. L. Rienks, Prof. J. Fink
Institute of Solid State Physics
Dresden University of Technology
Zellescher Weg 16, 01062 Dresden, Germany

Dr. J. L. Mañes
Condensed Matter Physics Department
Faculty of Science and Technology
University of the Basque Country UPV/EHU
Apdo. 644, 48080 Bilbao, Spain

Prof. S. S. P. Parkin
Max Planck Institute of Microstructure Physics
06120 Halle, Germany

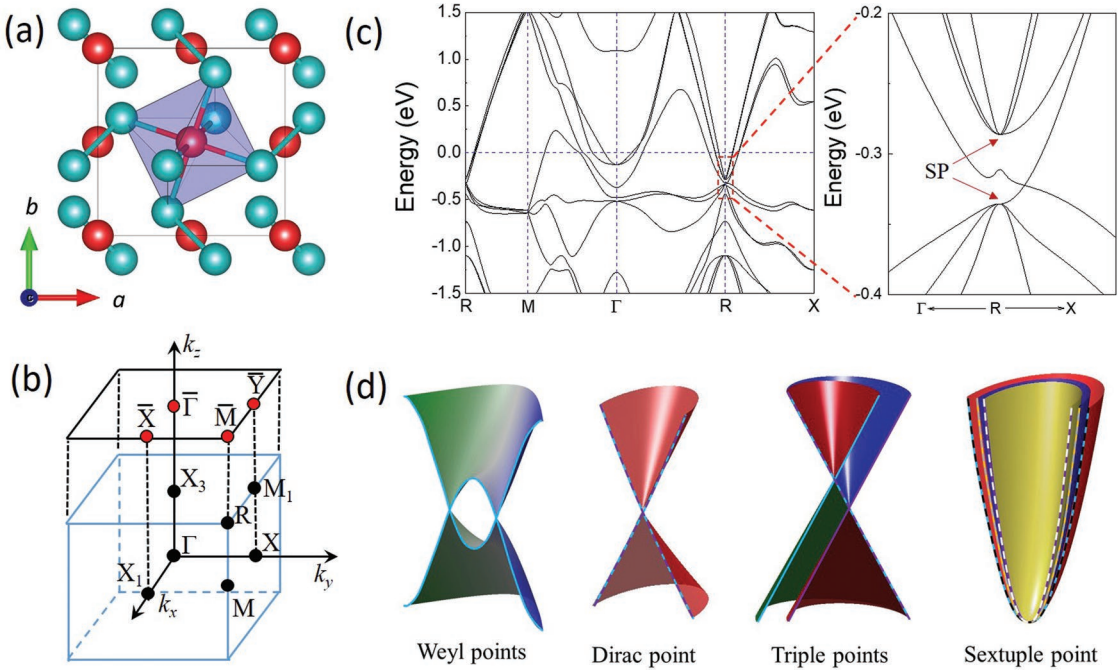

Figure 1. Crystal and band structures of $PdSb_2$. a) 3D crystal structure of $PdSb_2$ exhibiting pyrite-type structure. Blue and red atoms are Sb and Pb, respectively. b) 3D bulk Brillouin zone (BZ) and (001) surface BZ with the high symmetry points highlighted. c) Calculated band structure along *R*–*M*–*Γ*–*R*–*X*. Two sextuple points (SPs) are observed at the *R* point at −0.286 and −0.334 eV below the Fermi level, as indicated by red arrows in the magnified image on the right. d) Schematic representation of Weyl, Dirac, triple, and sextuple points.

focused on establishing the existence of surface Fermi arcs, which are a consequence of the large Chern number associated with the sixfold crossings in this space group. By contrast, here we show for the first time the existence of sextuple points that have a vanishing Chern number and are therefore expected to show no surface Fermi arcs. A schematic representation of Weyl, Dirac, triple, and sextuple points are shown in **Figure 1**d.

Sextuple points are formed by doubling the threefold degeneracies at the time-reversal invariant *R* point in the corner of the Brillouin zone (BZ).[22] Owing to its crystal symmetry, the nonmagnetic pyrite-type structure provides a unique opportunity to study sextuple point compounds. Compounds with such a structure have been extensively studied and have diverse properties ranging from semiconducting to superconductivity.[29,30] Recently, we reported that a superconducting transition temperature of up to 13.1 K could be achieved in the high pressure pyrite structure of $PdSe_2$.[31] Interestingly, many pyrite compounds have been identified for their topological features in the band structure. For example, the Dirac semimetal $PtBi_2$ can also exhibit sextuple points.[32] The isoelectronic metal $PdSb_2$ exhibits superconducting behavior below 1.25 K.[33] The electronic band structure of both these compounds is similar with an important difference, i.e., the sextuple point lies below the Fermi level in $PdSb_2$, whereas it lies much above in $PtBi_2$. Hence, $PdSb_2$ is a better candidate to investigate the novel sextuple point. Here, we have employed angle-resolved photoemission spectroscopy (ARPES), first principle calculations, and group theoretical analysis to verify the existence of this point in $PdSb_2$.

$PdSb_2$ crystallizes in the pyrite (FeS_2) structure which belongs to the space group $Pa\bar{3}$ (SG 205) with lattice parameters $a = b = c = 6.4616(4)$ Å determined from single crystal X-ray diffraction. The crystal structure of $PdSb_2$ is shown in Figure 1a, where Pd and Sb atoms occupy the Wyckoff positions 4*a* and 8*c*, respectively. The structure is composed of 2 distinct motifs, $PdSb_2$ dumbbells and $PdSb_6$ octahedra. The latter are significantly distorted so that C_4 rotational symmetry is lifted and thus, the *X* and *Y* points in the bulk BZ are inequivalent. Note that the *R* and *M* points in the bulk BZ are projected to the $\bar{M}$ point in the surface BZ (see Figure 1b). In Figure 1c, we show the calculated band structure of $PdSb_2$ along the high symmetry lines. All the bands are doubly degenerated due to the inversion center. $PdSb_2$ is metallic with several electron and hole bands. The most important feature of the band structure is at the *R* point, where two sextuple points appear below the Fermi energy (see inset of Figure 1c). Notably, the band dispersion is parabolic near the sextuple points. In the presence of time-reversal symmetry, the threefold degeneracy at the *R* point is doubled to give rise to sextuple point. We use group theoretical analysis to understand how the sextuple points are generated at the *R* point and how the bands split away from this point, which agrees with the orbital diagnosis from density functional theory (DFT) calculations (see Note S1 in the Supporting Information). The calculations, including spin–orbit coupling, further reveal that three twofold degenerate bands predominantly originate from Pd-d orbitals and Sb-p orbitals at the sextuple crossing point. For a comparison, we show the schematic representation of Weyl, Dirac, triple, and sextuple points in Figure 1d. In contrast to the well-known Weyl and Dirac semimetals, which exhibit twofold and fourfold degeneracies at the crossing point, respectively, a threefold degenerate point (triple point) originates from the crossing of a twofold and a nondegenerate band, which has been experimentally realized in symmorphic MoP.[24] However, unlike other topological semimetals, $PdSb_2$ exhibits sixfold band crossings.

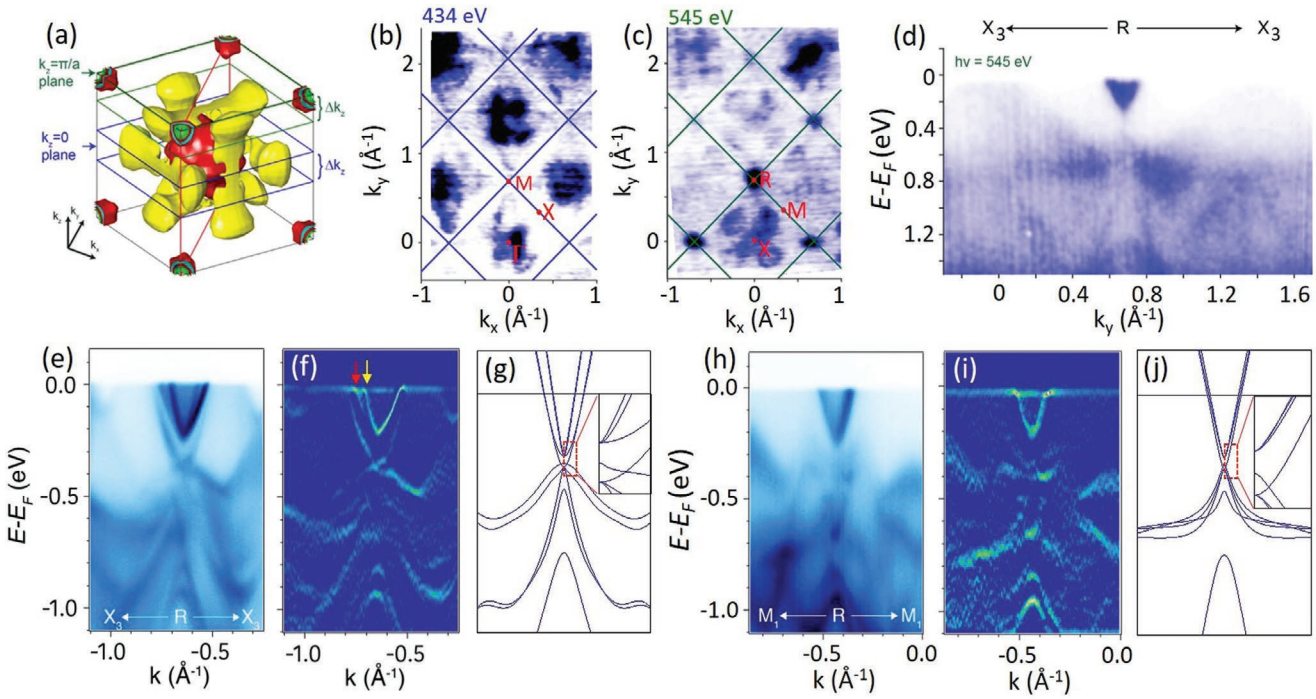

Figure 2. Electronic structure of $PdSb_2$. a) Calculated 3D Fermi surface, indicating the high symmetry planes and broadening along k_z by blue, green, and red lines. b) Measured Fermi surface in the $k_z = 0$ plane, measured with photon energy 434 eV. c) Measured Fermi surface in the $k_z = \pi/a$ plane, measured with photon energy 545 eV. d) Measured band dispersion along the X_3–R–X_3 direction, at the photon energy 545 eV. e) Measured band dispersion along the X_3–R–X_3 direction, at the photon energy 65 eV. f) The corresponding curvature intensity plot. g) Calculated band structure along X_3–R–X_3. Inset shows the magnified view near the sextuple point. h–j) ARPES intensity plot, the corresponding curvature intensity plot, and the calculated band structure along M_1–R–M_1.

The sixfold degenerate points at the corner of the Brillouin zone, R point in $PdSb_2$ is invariant under time reversal symmetry. The combination of the time reversal symmetry and the inversion symmetry from the crystal structure gives the quadratic nature of the bands at the sixfold crossing point which lacks the net berry curvature and topological surface states. However, the recent quantum oscillation studies under the magnetic field (upon breaking the time reversal symmetry) suggest a nontrivial character of the bands with a π-Berry phase.[34] This can also be a reminiscent of the band inversion between the two pairs of sixfold degenerate points at the R point presented in Note S1 (Supporting Information).

We implemented ARPES technique to verify the existence of sextuple points experimentally, which is complemented by first principle calculations. We performed k_z-dependent measurement (Figure S1, Supporting Information) and Fermi surface (FS) mapping. We acquired the FS of $PdSb_2$ with 434 and 545 eV light, which represents $k_z = 0$ and π, respectively (**Figure 2**b,c). Figure 2a shows the calculated 3D FS of $PdSb_2$. The cross-like structure at the $\bar{\Gamma}$ point is formed by three hole pockets. In total, four electron pockets are located at $\bar{M}$ points. Among them, three inner degenerate bands form the upper sextuple point. In addition to the cross-like structure in the center, Figure 2c also shows elliptical electron pockets at corners of each BZs (R points). The calculated 3D FS is in good agreement with the experimental FS. Figure 2d shows the band dispersion around R point measured using 545 eV light, indicating the presence of crossing point below fermi energy, however with a low resolution.

In order to achieve high in-plane resolution around the sixfold band crossing, we performed detailed investigation of the electronic structure near the R point with ultraviolet light. The band dispersion near this point (along the X_3–R–X_3 direction) is measured with 65 eV p-polarized photon (Figure 2e), which reveals the presence of two concentric electron pockets centered at R. These pockets coincide with each other at the upper sixfold degenerate point, which appears at ≈0.25 eV binding energy. Compared to the calculations, the Fermi energy shows a rigid shift of ≈0.036 eV in our measurements. These two bands are clearly resolved in the curvature intensity plot (Figure 2f), which are marked by yellow and red arrows. The experimental k_F values relative to the R point of the inner and outer electron pockets are 0.1 and 0.19 Å^{-1}, respectively. Further, we investigated the band dispersion along the M_1–R–M_1 direction (Figure 2h) with 65 eV p-polarized light, which also indicated electron pockets at R point. However, it is difficult to discern them separately through the curvature intensity plot along the M_1–R–M_1 direction (Figure 2i).

Comparing the ARPES data with that obtained using ab initio calculations, we observe that the bottom of the two parabolic crossing bands is a crossing of three bands, resulting in a sextuple point. Figure 2g shows the theoretically calculated band structure along X_3–R–X_3. Although the agreement between the experimental and calculated band structure is

quite good, we find that the single band denoted by the yellow arrow (the inner parabolic band) in the intensity curvature plot is in fact a combination of two bands. It is evident from the magnified version of the calculated data at the R point (inset of Figure 2g) that these bands are barely separated in momentum. Therefore, it is impossible to resolve them by ARPES. Although, we cannot resolve the predicted band splitting due to band broadening, the overall agreement between our ARPES data and band structure calculations suggests the existence of the sextuple crossings at the R point. We also see the evidence of the lower sextuple point at ≈–0.38 eV (see Figure S3 in the Supporting Information for the details). We show the calculated band structure along M_1–R–M_1 in Figure 2j. The slight disagreement between the experimental and calculated band structure in this direction occurs due to the partial integration of intensity along k_z that has been made to the experimental data. However, we observe a reasonable agreement when the calculation is carried out from $k_z = 0$ to π with a step size of 0.2π (Figure S5, Supporting Information). The magnified band dispersion in this direction is shown in the inset of Figure 2j. Using group theory and ab initio calculations (Note S1, Supporting Information), we prove that a band inversion takes place between the two sixfold of the $\bar{R}_{10}\bar{R}_{10}$ and $\bar{R}_{11}\bar{R}_{11}$ irreducible representations from different elementary band representations (representing d and p orbitals, respectively).

As shown in **Figure 3**a, the three parabolic electron bands that constitute a sextuple point are asymmetric. We follow these bands across the sextuple point by measuring constant energy surfaces. Figure 3b,c shows the experimental and theoretically calculated constant energy surfaces of $PdSb_2$, respectively. The lower sextuple point at $\bar{M}$ point (R point in the bulk is projected at $\bar{M}$ of the surface BZ) is formed from the degeneracy of the three electron pockets (Figure 3d). As mentioned earlier, the FS of $PdSb_2$ exhibits a "cross-"shaped structure at the $\bar{\Gamma}$ point and elliptical electron pockets at the $\bar{M}$ point. As the binding energy increases, the size of the hole pockets at the $\bar{\Gamma}$ point increases, while the size of the electron pockets at the $\bar{M}$ point continuously decreases and, finally, shrinks to the upper sextuple point ≈–0.286 eV (corresponding to –0.25 eV in ARPES), which is denoted by a dot.

Polarization-dependent ARPES spectra measured with p-polarized photons along X_3–R–X_3 reveal the presence of two bands (**Figure 4**a), which is also evident in the momentum distribution curves shown in Figure 4b. The ab initio calculations indicate that Pd-d and Sb-p orbitals contribute predominantly to the sextuple point. All the d-bands are strongly hybridized and the even parity orbitals (with respect to the sample and detector geometry in the ARPES experiments) primarily contribute in the p-polarization measurements. ARPES spectra measured with linear s-polarized photons (Figure 4b) also exhibit two bands, which have predominant contributions from odd parity Pd-d orbitals. The observation of two bands in both polarization measurements is the experimental proof of a strong hybridization of the d orbitals.

In conclusion, ARPES measurements provide a clear experimental signature of six component fermions in $PdSb_2$. This investigation will stimulate further studies in identifying novel fermions with quadratic band crossings, which can exhibit unusual physical properties that are distinctly different from that of Dirac and Weyl fermions. In $PdSb_2$, the sextuple point is situated too far below the Fermi energy (≈0.25 eV) to much influence its transport properties. Interestingly, the sextuple point is predicted to occur just above the Fermi energy in the isoelectronic and isostructural $PtBi_2$. Thus, a solid solution of $PdSb_2$ and $PtBi_2$ could be an ideal candidate to identify sextuple

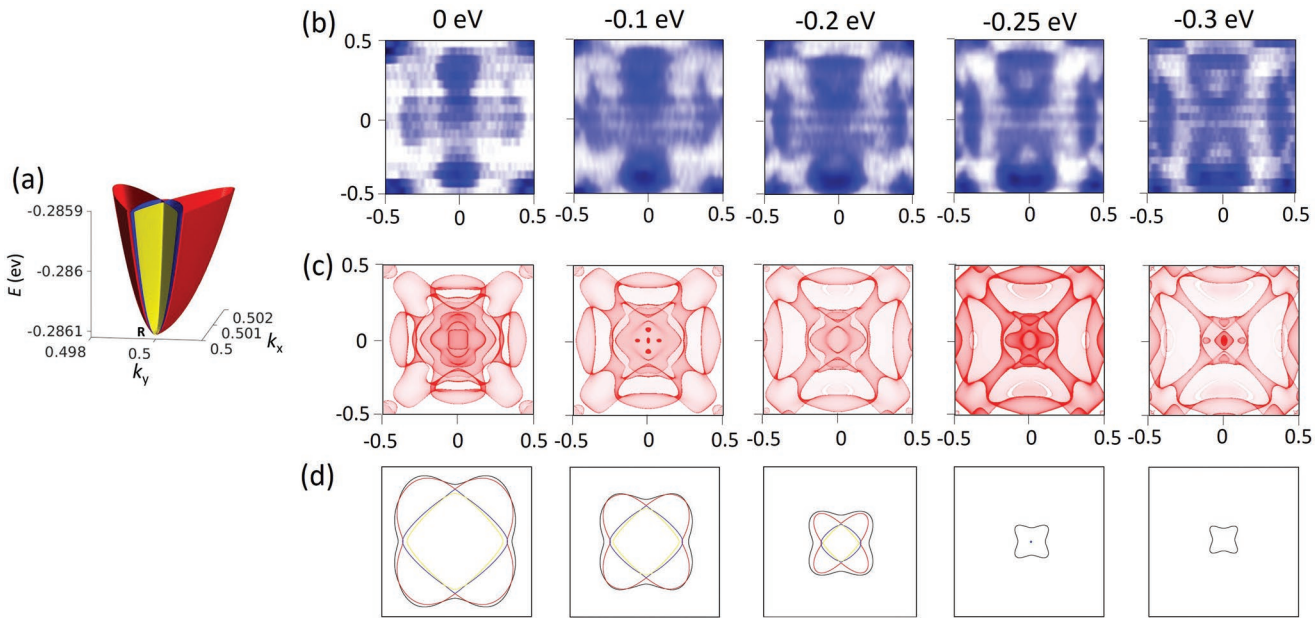

Figure 3. Band evolution and constant energy surfaces. a) Parabolic bands constituting the sextuple point. The outermost band is more asymmetric as compared to the two inner bands. b) Experimental constant energy surfaces of $PdSb_2$ at E_F 0, –0.1, –0.2, –0.25, and –0.3 eV. c) Calculated constant energy surfaces corresponding to (b). d) Calculated band evolution around the sextuple point. The sextuple point at ≈–0.25 eV is denoted by a dot.

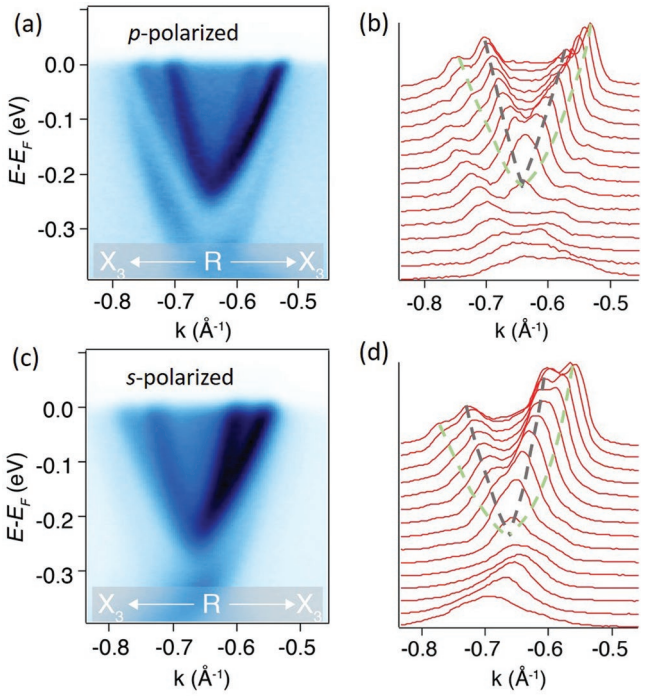

Figure 4. ARPES spectra and momentum distribution curves. a) ARPES spectra measured with 65 eV p-polarized photons, b) the corresponding momentum distribution curves overlapped with dashed lines, representing the projected peak positions. c,d) The corresponding data acquired with s-polarized photons at the same energy.

Fermions from transport studies. Our calculations and experimental data support the presence of electron and hole pockets in the Brillouin zone of $PdSb_2$. The carrier compensation thus provided can give rise to parabolic and unsaturated magnetoresistance, which is consistent with the transport properties observed in ref. [34]. The nontrivial π-Berry phase observed in the quantum oscillations studies by Chapai et al.[34] makes a strong case for a topological phase transition of the sextuple point under strong magnetic field. This calls for elaborated experimental and theoretical studies on compounds containing sextuple points. Furthermore, $PdSb_2$ is a superconducting pyrite with a d^6 metal configuration.[34] We believe that this is the first study to demonstrate the existence of a sextuple point below the Fermi energy in a superconducting pyrite. Therefore, $PdSb_2$ is an interesting test bed to understand the superconducting instabilities of exotic fermions, which could open new routes toward unconventional superconducting states of matter.

Experimental Section

Single Crystal Growth: $PdSb_2$ single crystals were grown by a flux method using excess Sb. In a typical synthesis, Pd and Sb pieces were weighed according to the composition $Pd_{30}Sb_{70}$ and transferred to an alumina crucible, which was then sealed in an evacuated quartz tube. The sealed tube was heated to 1000 °C at a rate of 100 °C h^{-1} and was kept at this temperature for 24 h. The temperature was gradually decreased to 750 °C in 5 h and then to 630 °C at a slow rate of 1 °C h^{-1}. At this temperature, the excess Sb was decanted off and the heating was switched off. The structure of the crystals and the sample composition were validated by Laue X-ray diffraction and X-ray energy dispersive analysis, respectively.

ARPES Measurements: Vacuum-ultraviolet-ARPES measurements were carried out at the UE112-PGM2b beamline of the synchrotron radiation facility BESSY (Berlin) using 1^2 and 1^3 end stations that were equipped with R8000 and R4000 analyzers, respectively. The sample was cleaved in situ at 35 K. All measurements were performed at temperatures ranging from 20 to 35 K and photon energies from 60 to 100 eV using both p- and s-polarizations. The total energy resolution was ≈15 meV and the angular resolution was 0.2°. Soft X-ray-ARPES measurements were performed at the ADRESS beamline installed at the Swiss Light Source. Samples were cleaved and measured at 15 K.

Band Structure Calculations: The electronic band structure was calculated ab initio using density functional theory with the full-potential local-orbital minimum-basis DFT code of FPLO.[35] The exchange and correlation energies were considered at the level of the generalized gradient approximation.[36] In all the calculations, the experimentally measured lattice structures were used. The Bloch wave function was projected into atomic-orbital-like Wannier functions. The k_z-projected Fermi surfaces were constructed from the tight-binding model Hamiltonian using the iterative Green's function method.[37,38]

Supporting Information

Supporting Information is available from the Wiley Online Library or from the author.

Acknowledgements

N.K., M.Y., J.N., M.G.V., and J.B. contributed equally to this work. This work was financially supported by the ERC Advanced Grant No. 742068 ("TOPMAT").

Conflict of Interest

The authors declare no conflict of interest.

Keywords

angle-resolved photoemission spectroscopy, electronic structure, first principle calculations, multifold degenerate points, topological materials

Received: September 15, 2019
Revised: December 24, 2019
Published online: February 9, 2020

[1] F. Wilczek, *Phys. Today* **1998**, *51*, 11.
[2] K. S. Novoselov, A. K. Geim, S. V. Morozov, D. Jiang, M. I. Katsnelson, I. V. Grigorieva, S. V. Dubonos, A. A. Firsov, *Nature* **2005**, *438*, 197.
[3] Z. Wang, Y. Sun, X.-Q. Chen, C. Franchini, G. Xu, H. Weng, X. Dai, Z. Fang, *Phys. Rev. B* **2012**, *85*, 195320.
[4] Z. K. Liu, B. Zhou, Y. Zhang, Z. J. Wang, H. M. Weng, D. Prabhakaran, S. K. Mo, Z. X. Shen, Z. Fang, X. Dai, Z. Hussain, Y. L. Chen, *Science* **2014**, *343*, 864.
[5] Z. K. Liu, J. Jiang, B. Zhou, Z. J. Wang, Y. Zhang, H. M. Weng, D. Prabhakaran, S. K. Mo, H. Peng, P. Dudin, T. Kim, M. Hoesch, Z. Fang, X. Dai, Z. X. Shen, D. L. Feng, Z. Hussain, Y. L. Chen, *Nat. Mater.* **2014**, *13*, 677.

[6] X. Wan, A. M. Turner, A. Vishwanath, S. Y. Savrasov, *Phys. Rev. B* **2011**, *83*, 205101.
[7] H. Weng, C. Fang, Z. Fang, B. A. Bernevig, X. Dai, *Phys. Rev. X* **2015**, *5*, 011029.
[8] S.-Y. Xu, I. Belopolski, N. Alidoust, M. Neupane, G. Bian, C. Zhang, R. Sankar, G. Chang, Z. Yuan, C.-C. Lee, S.-M. Huang, H. Zheng, J. Ma, D. S. Sanchez, B. Wang, A. Bansil, F. Chou, P. P. Shibayev, H. Lin, S. Jia, M. Z. Hasan, *Science* **2015**, *349*, 613.
[9] Z. K. Liu, L. X. Yang, Y. Sun, T. Zhang, H. Peng, H. F. Yang, C. Chen, Y. Zhang, Y. F. Guo, D. Prabhakaran, M. Schmidt, Z. Hussain, S. K. Mo, C. Felser, B. Yan, Y. L. Chen, *Nat. Mater.* **2016**, *15*, 27.
[10] N. P. Armitage, E. J. Mele, A. Vishwanath, *Rev. Mod. Phys.* **2018**, *90*, 015001.
[11] T. Liang, Q. Gibson, M. N. Ali, M. Liu, R. J. Cava, N. P. Ong, *Nat. Mater.* **2015**, *14*, 280.
[12] C. Shekhar, A. K. Nayak, Y. Sun, M. Schmidt, M. Nicklas, I. Leermakers, U. Zeitler, Y. Skourski, J. Wosnitza, Z. Liu, Y. Chen, W. Schnelle, H. Borrmann, Y. Grin, C. Felser, B. Yan, *Nat. Phys.* **2015**, *11*, 645.
[13] T. Liang, J. Lin, Q. Gibson, S. Kushwaha, M. Liu, W. Wang, H. Xiong, J. A. Sobota, M. Hashimoto, P. S. Kirchmann, Z.-X. Shen, R. J. Cava, N. P. Ong, *Nat. Phys.* **2018**, *14*, 451.
[14] E. Liu, Y. Sun, N. Kumar, L. Muechler, A. Sun, L. Jiao, S.-Y. Yang, D. Liu, A. Liang, Q. Xu, J. Kroder, V. Süß, H. Borrmann, C. Shekhar, Z. Wang, C. Xi, W. Wang, W. Schnelle, S. Wirth, Y. Chen, S. T. B. Goennenwein, C. Felser, *Nat. Phys.* **2018**, *14*, 1125.
[15] C. Shekhar, N. Kumar, V. Grinenko, S. Singh, R. Sarkar, H. Luetkens, S.-C. Wu, Y. Zhang, A. C. Komarek, E. Kampert, Y. Skourski, J. Wosnitza, W. Schnelle, A. McCollam, U. Zeitler, J. Kübler, B. Yan, H. H. Klauss, S. S. P. Parkin, C. Felser, *Proc. Natl. Acad. Sci. USA* **2018**, *115*, 9140.
[16] J. Xiong, S. K. Kushwaha, T. Liang, J. W. Krizan, M. Hirschberger, W. Wang, R. J. Cava, N. P. Ong, *Science* **2015**, *350*, 413.
[17] X. Huang, L. Zhao, Y. Long, P. Wang, D. Chen, Z. Yang, H. Liang, M. Xue, H. Weng, Z. Fang, X. Dai, G. Chen, *Phys. Rev. X* **2015**, *5*, 031023.
[18] M. Hirschberger, S. Kushwaha, Z. Wang, Q. Gibson, S. Liang, C. A. Belvin, B. A. Bernevig, R. J. Cava, N. P. Ong, *Nat. Mater.* **2016**, *15*, 1161.
[19] C. Zhang, Y. Zhang, X. Yuan, S. Lu, J. Zhang, A. Narayan, Y. Liu, H. Zhang, Z. Ni, R. Liu, E. S. Choi, A. Suslov, S. Sanvito, L. Pi, H.-Z. Lu, A. C. Potter, F. Xiu, *Nature* **2019**, *565*, 331.
[20] F. Tang, Y. Ren, P. Wang, R. Zhong, J. Schneeloch, S. A. Yang, K. Yang, P. A. Lee, G. Gu, Z. Qiao, L. Zhang, *Nature* **2019**, *569*, 537.
[21] A. A. Soluyanov, D. Gresch, Z. Wang, Q. Wu, M. Troyer, X. Dai, B. A. Bernevig, *Nature* **2015**, *527*, 495.
[22] B. Bradlyn, J. Cano, Z. Wang, M. G. Vergniory, C. Felser, R. J. Cava, B. A. Bernevig, *Science* **2016**, *353*, aaf5037.
[23] Z. Zhu, G. W. Winkler, Q. Wu, J. Li, A. A. Soluyanov, *Phys. Rev. X* **2016**, *6*, 031003.
[24] B. Q. Lv, Z. L. Feng, Q. N. Xu, X. Gao, J. Z. Ma, L. Y. Kong, P. Richard, Y. B. Huang, V. N. Strocov, C. Fang, H. M. Weng, Y. G. Shi, T. Qian, H. Ding, *Nature* **2017**, *546*, 627.
[25] J. Z. Ma, J. B. He, Y. F. Xu, B. Q. Lv, D. Chen, W. L. Zhu, S. Zhang, L. Y. Kong, X. Gao, L. Y. Rong, Y. B. Huang, P. Richard, C. Y. Xi, E. S. Choi, Y. Shao, Y. L. Wang, H. J. Gao, X. Dai, C. Fang, H. M. Weng, G. F. Chen, T. Qian, H. Ding, *Nat. Phys.* **2018**, *14*, 349.
[26] D. S. Sanchez, I. Belopolski, T. A. Cochran, X. Xu, J.-X. Yin, G. Chang, W. Xie, K. Manna, V. Süß, C.-Y. Huang, N. Alidoust, D. Multer, S. S. Zhang, N. Shumiya, X. Wang, G.-Q. Wang, T.-R. Chang, C. Felser, S.-Y. Xu, S. Jia, H. Lin, M. Z. Hasan, *Nature* **2019**, *567*, 500.
[27] Z. Rao, H. Li, T. Zhang, S. Tian, C. Li, B. Fu, C. Tang, L. Wang, Z. Li, W. Fan, J. Li, Y. Huang, Z. Liu, Y. Long, C. Fang, H. Weng, Y. Shi, H. Lei, Y. Sun, T. Qian, H. Ding, *Nature* **2019**, *567*, 496.
[28] N. B. M. Schröter, D. Pei, M. G. Vergniory, Y. Sun, K. Manna, F. de Juan, J. A. Krieger, V. Süss, M. Schmidt, P. Dudin, B. Bradlyn, T. K. Kim, T. Schmitt, C. Cacho, C. Felser, V. N. Strocov, Y. Chen, *Nat. Phys.* **2019**, *15*, 759.
[29] F. Hulliger, E. Mooser, *J. Phys. Chem. Solids* **1965**, *26*, 429.
[30] F. Hulliger, J. Müller, *Phys. Lett.* **1963**, *5*, 226.
[31] M. A. ElGhazali, P. G. Naumov, H. Mirhosseini, V. Süß, L. Müchler, W. Schnelle, C. Felser, S. A. Medvedev, *Phys. Rev. B* **2017**, *96*, 060509.
[32] W. Gao, N. Hao, F.-W. Zheng, W. Ning, M. Wu, X. Zhu, G. Zheng, J. Zhang, J. Lu, H. Zhang, C. Xi, J. Yang, H. Du, P. Zhang, Y. Zhang, M. Tian, *Phys. Rev. Lett.* **2017**, *118*, 256601.
[33] B. T. Matthias, T. H. Geballe, V. B. Compton, *Rev. Mod. Phys.* **1963**, *35*, 1.
[34] R. Chapai, Y. Jia, W. A. Shelton, R. Nepal, M. Saghayezhian, J. F. DiTusa, E. W. Plummer, C. Jin, R. Jin, *Phys. Rev. B* **2019**, *99*, 161110.
[35] G. Kresse, J. Furthmüller, *Phys. Rev. B* **1996**, *54*, 11169.
[36] J. P. Perdew, K. Burke, M. Ernzerhof, *Phys. Rev. Lett.* **1996**, *77*, 3865.
[37] M. P. L. Sancho, J. M. L. Sancho, J. Rubio, *J. Phys. F: Met. Phys.* **1984**, *14*, 1205.
[38] M. P. L. Sancho, J. M. L. Sancho, J. Rubio, *J. Phys. F: Met. Phys.* **1985**, *15*, 851.